

Deformable Registration of CT Pelvis Images Using Mjolnir

Lotta M. Ellingsen and Jerry L. Prince

The Johns Hopkins University
Image Analysis and Communications Lab
105 Barton Hall, 3400 N. Charles Street, Baltimore, MD 21218
USA
E-mail: lotta@jhu.edu, prince@jhu.edu
URL: <http://www.iacl.ece.jhu.edu>

ABSTRACT

Our recently published 3D-3D deformable image registration algorithm, *Mjolnir* (Ellingsen et al., 2006) was developed for inter-subject registration of MR brain images. *Mjolnir* is a hybrid registration method, where both anatomical features and image intensities are used to hierarchically align the images. In addition to the hierarchical scheme, the algorithm was implemented in a multi-resolution framework, which both reduces local minima and speeds up the registration process. In this paper an extension to this work is proposed, where *Mjolnir* has been adapted to register CT images of the pelvis. The main concepts of *Mjolnir* will be briefly described and the changes made to previous work explained. The algorithm was tested on CT images of the pelvis of 13 different subjects. Results indicate good registration accuracy however, further validation is needed.

1. INTRODUCTION

Deformable inter-subject image registration is the process of spatially aligning images of different subjects into a common reference frame so that they can be compared either visually or statistically. During the last few years the need for development of different deformable registration methods has emerged from different clinical applications, such as longitudinal studies and surgical planning [1–7]. The motivation for the extension to our work from MR brain images to CT pelvis images was the need in our research group to create an anatomical atlas for atlas assisted tomography. The proposed registration method was used to register a set of CT images. The resulting displacement fields were then used to align 3D tetrahedral meshes of the subjects to build a statistical anatomical atlas for compensation of missing views in a limited angle cone-beam trajectory [8].

In this paper the basic principles of our previous work on 3D-3D deformable registration of MR brain images [7], upon which this paper builds, will be reviewed. Modifications made to adapt the algorithm to deal with CT pelvis images will be explained and results of the proposed registration method shown.

This work was supported in part by NIH/NIBIB Grant 1R21EB003616

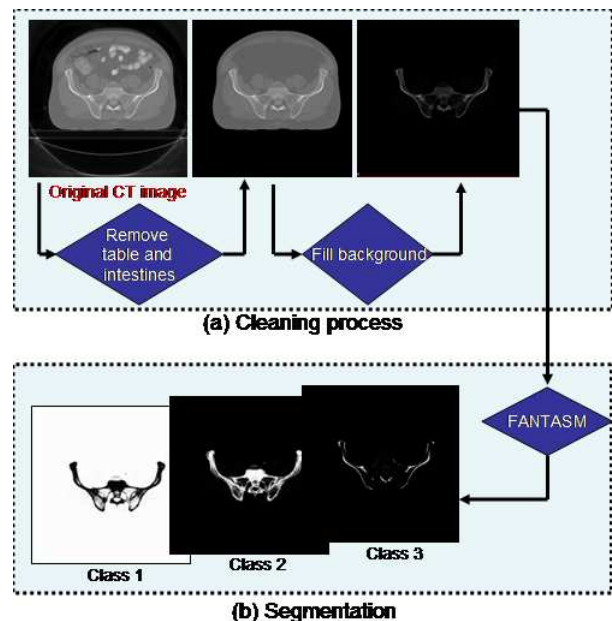


Fig. 1. Pre-processing of the CT data to remove irrelevant elements from the image and segment the bone.

2. METHOD

2.1. Pre-processing

CT images not only contain objects of interest but also some background elements, like the scanner table. Since our algorithm is based on feature selection and alignment, it was preferred not to have the program spend time aligning features that were irrelevant to our research purpose. Therefore, all such background features were eliminated from the images (see Fig. 1a). Furthermore, since the ultimate objective of our work was to use the results to generate a pelvic bone atlas, the strong edge feature between the background and the soft tissue of the patient was removed. This also led to better registration results of the bone because of the challenge of allowing large displacements in the soft tissue while maintaining more rigidity in the bone structure due to much smaller variability in bone tissue size compared to soft tissue size (see Fig. 2). Fi-

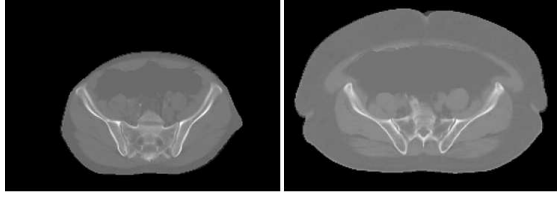


Fig. 2. High variability in soft tissue compared to bone tissue between different subjects.

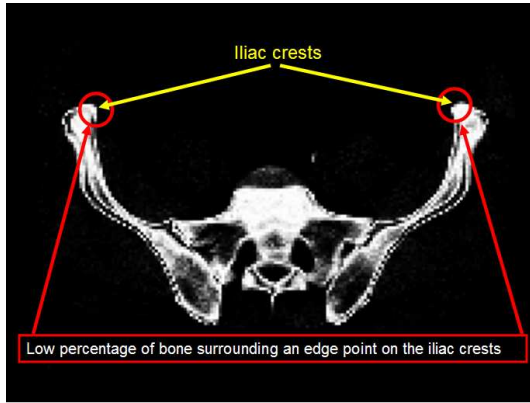


Fig. 3. Demonstration of primary driving voxel selection on the second class image from the fuzzy segmentation. Small bone volume is contained in spherical neighborhoods around edge points on high curvature regions like the iliac crests.

nally, because of the high deformability and thus extreme shape difference of the intestines between different subjects, the intestines were eliminated from the images as well. The complete cleaning process was performed by filling the background and all unwanted elements of the image with approximate soft tissue values, which produced a nice segmentation of the bone from its surroundings (see Fig. 1a). After the cleaning process the images were segmented into three membership classes, approximately corresponding to background (class 1), marrow (class 2), and bone (class3) (see Fig. 1b). The Fuzzy And Noise Tolerant Adaptive Segmentation Method (FANTASM) [9, 10] was utilized in the segmentation process. The three classified images are the base of the feature extraction of our registration algorithm (section 2.2). A demonstration of the complete pre-processing procedure is shown on Fig. 1.

2.2. Attribute Vectors and Driving Voxels

Two of the most important elements of Mjolnir are attribute vectors and driving voxels. Information about the image intensity and derived local features are concatenated into an attribute vector, which is computed at every voxel of both the template and subject images. The vector consists of three parts. The first part is a 1×1 vector that represents the edge type of the voxel, the second part is a 1×1 vector of the voxel's CT image intensity, and the third part is a

9×1 vector of geometric moment invariants (GMIs). The GMIs are formulated from the zero-order and second-order 3D regular moments in the following way:

$$\begin{aligned} I_1 &= M_{0,0,0} \\ I_2 &= M_{2,0,0} + M_{0,2,0} + M_{0,0,2} \\ I_3 &= M_{2,0,0} \times M_{0,2,0} + M_{2,0,0} \times M_{0,0,2} \\ &\quad + M_{0,2,0} \times M_{0,0,2} - M_{1,0,1}^2 - M_{1,1,0}^2 - M_{0,1,1}^2, \end{aligned}$$

where

$$M_{p,q,r} = \iiint_{(x_1)^2+(x_2)^2+(x_3)^2 < R_G^2} x_1^p x_2^q x_3^r f_m(x_1, x_2, x_3) dx_1 dx_2 dx_3$$

is the $(p+q+r)$ -th 3D regular moment and f_m is one of the membership class images (as in Fig. 1b). The three GMIs, I_1 , I_2 , and I_3 , are computed on a spherical neighborhood of radius R_G around each voxel for each of the three membership classes based on the fuzzy segmentation of the image. This combination of derived image features and the original image intensities gives a rich enough attribute vector to locally represent the underlying anatomy of each voxel and make it possible to automatically find correspondence between the two images.

When an attribute vector has been computed for every voxel in both the template and subject images, distinctive driving voxels can be automatically identified. These are the landmark points that drive the registration process. The driving voxels are hierarchically selected such that strong, reliable features are aligned first. On MR brain images such points are located on the highly convoluted brain cortex [7]. On CT pelvis images on the other hand, such primary driving voxels are located on high curvature points on the bone, such as the iliac crests. Therefore, one of the main modifications to be made from our previous work was to adjust the driving voxel criteria.

There are two main reasons why voxels on regions like the iliac crests have distinctive attribute vectors. First, if we consider the second class image from the fuzzy segmentation we can see that they have high curvature and that therefore there is a small bone volume within a spherical neighborhood around an edge point on the iliac crests (see Fig. 3). This property is represented by the first GMI, I_1 . The I_1 -image for each class contains the segmented image after filtration by an average filter with a spherical mask. Hence, this element of the attribute vector can be used to automatically identify distinct and reliable primary driving voxels. Second, the number of voxels that belong to the iliac crests is relatively small compared to other pelvic voxels, so only a few voxels in their neighborhood will be good matching candidates. After aligning the primary driving voxels, more voxels are gradually added to the set of driving voxels until every voxel in the template image becomes

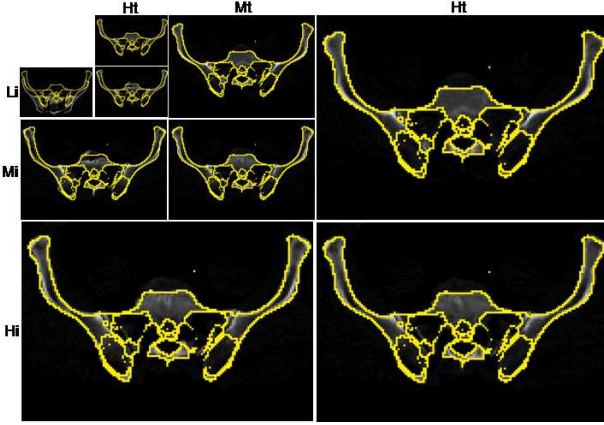


Fig. 4. This figure demonstrates the multi-resolution scheme in Mjolnir and shows results from registering two real CT images using the new algorithm. Li, Mi, and Hi are the input images for low, middle, and high resolution respectively. Lt, Mt, and Ht are the template images at the corresponding resolutions. The bottom right image in each set of three is the result for each resolution. The yellow lines are the same on all the images and are displayed for reference. They represent the outline of the first class from the segmentation of the template image.

a driving voxel in the last few iterations. This hierarchical strategy minimizes the number of sub-optimal correspondences at an early state in the registration process and makes the algorithm more robust.

2.3. Correspondences and Feature Diffusion

Once driving voxels have been selected the next step is to find landmark correspondences from which to drive the registration process. Correspondences are found for every driving voxel by comparing attribute vectors and minimizing their similarity between matching voxels. Both the template and subject images have driving voxels and therefore, the matching is performed in two directions, i.e., from template to subject and vice versa, which makes the correspondences more consistent. However, the displacement vectors are all defined in the domain of the template, which means that if one template driving voxel has two different displacement vectors attached to it (i.e., one from each directional matching process), these vectors are combined to generate one final displacement field in the domain of the template.

Because of the hierarchical driving voxel scheme a very important next step is to interpolate the derived displacement vectors to produce a smooth displacement field for every voxel in the image. This is done by using the displacement vectors as constraints in a partial differential equation (PDE). A fast multi-grid method [11] was used to solve the PDE

$$g\nabla^2\mathbf{v} - p(\mathbf{v} - \mathbf{u}) = \mathbf{0}, \quad (1)$$

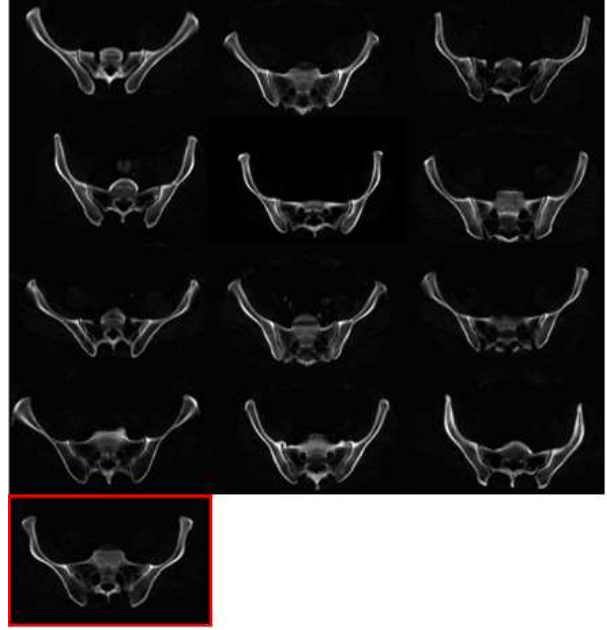


Fig. 5. A total of 12 different subjects selected for validation study. The template image is shown in the red box.

where $\nabla^2 = \partial^2/\partial x^2 + \partial^2/\partial y^2 + \partial^2/\partial z^2$ is the Laplacian operator, \mathbf{v} is the interpolated displacement field, and \mathbf{u} is the initial, sparse displacement field computed from the correspondences at the driving voxels. The scalar functions p and g are weighting functions that control the closeness of the displacement field \mathbf{v} to the correspondence field \mathbf{u} and the smoothness of \mathbf{v} , respectively. The equilibrium solution \mathbf{v} provides a displacement field, which is allowed to follow the displacement vectors closely where there are many strong reliable feature matches (like the iliac crest), while producing a smooth displacement field elsewhere. The smoothing control, g , was set to be higher throughout the registration process for bone images than for brain images, since the bone has bulkier flat surfaces than the brain.

2.4. Multi-resolution Scheme

In order to allow larger displacements and to speed up convergence the algorithm was implemented in a multi-resolution framework. First, the images were downsampled by a factor of four and the registration procedure run until the algorithm converged. Then the resulting displacement field was upsampled to generate an input image for the next resolution. This procedure was repeated for three resolutions until the final result had the same resolution as the original images. This is demonstrated in Fig. 4. A global alignment was achieved after the low resolution registration and then fine details were captured on the higher resolution results.

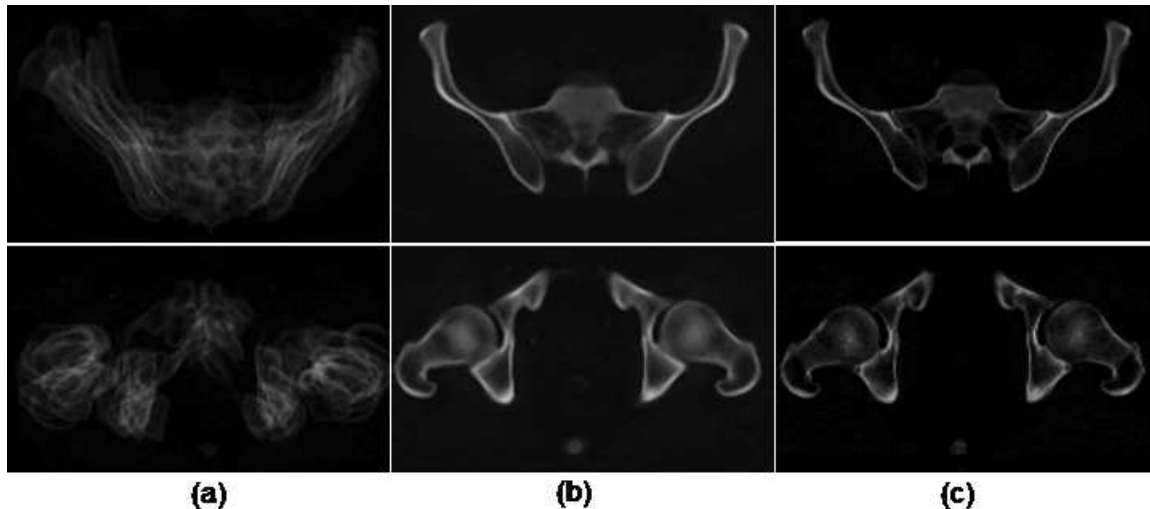


Fig. 6. Average of 12 pelvis images (a) before registration (b) after registering each image to a template image using the modified Mjolnir algorithm. (c) Template image. Two different axial slices are shown.

3. RESULTS

The average of deformed images is often used to visually assess the accuracy of registration algorithms. A total of 12 CT images of the pelvis with variability in shape and size were selected (see Fig. 5). The modified Mjolnir algorithm was then used to register them all to a 13th template image and the average of the 12 warped images computed. Fig. 6 shows two different slices of the average of the 12 images both before and after the registration. In comparison, the corresponding slices of the template image are shown as well. The average image after registration is quite sharp and even the smallest details from the template image are visible on the average image, which is an indication of good accuracy of our algorithm.

4. CONCLUSIONS

The 3D-3D deformable registration algorithm Mjolnir was modified to be able to register CT images of the pelvis. A total of 12 subject images with high variability in shape and size were selected for a validation study of the modified algorithm. The proposed method was used to register the images to a 13th template image and the average of the warped images computed. The results indicate high registration accuracy however, further validation studies on the performance of our algorithm in registering pelvis images is needed. In future work, the algorithm could be extended to be able to capture large deformations in highly deformable soft tissue while maintaining more rigidity in the bone tissue of the pelvis.

5. REFERENCES

[1] D. Rueckert, L. I. Sonoda, C. Hayes, D. L. G. Hill, M. O. Leach, and D. J. Hawkes, "Nonrigid registration using free-form deforma-

tions: Application to breast MR images," *IEEE Trans. Med. Imag.*, vol. 18(8), pp. 712–721, 1999.

- [2] D. Shen and C. Davatzikos, "HAMMER: Hierarchical attribute matching mechanism for elastic registration," *IEEE Trans. Med. Imag.*, vol. 21(11), pp. 1421–1439, 2002.
- [3] G. K. Rohde, A. Aldroubi, and B. M. Dawant, "The adaptive bases algorithm for intensity-based nonrigid image registration," *IEEE Trans. Med. Imag.*, vol. 22(11), pp. 1470–1479, 2003.
- [4] Dinggang Shen, "Image registration by hierarchical matching of local spatial intensity histograms," in *The Seventh Annual International Conference on Medical Image Computing and Computer-Assisted Intervention (MICCAI)*, 2004, pp. 582–590.
- [5] Y. Zhan, D. Shen, and R. H. Taylor, "Deformable registration of male pelvises in CT images," in *IEEE International Symposium on Biomedical Imaging (ISBI)*, 2004, pp. 1463–1466.
- [6] He Wang, Lei Dong, Jennifer O'Daniel, Radhe Mohan, Adam S Garden, K Kian Ang, Deborah A Kuban, Mark Bonnen, Joe Y Chang, and Rex Cheung, "Validation of an accelerated 'demons' algorithm for deformable image registration in radiation therapy," *Physics in Medicine and Biology*, vol. 50, no. 12, pp. 2887–2905, 2005.
- [7] L. M. Ellingsen and J. L. Prince, "Mjolnir: Deformable image registration using feature diffusion," in *Proceedings of the SPIE Medical Imaging Conference*, 2006, vol. 6144, pp. 329–337.
- [8] O. Sadowsky, K. Ramamurthi, L. M. Ellingsen, G. Chintalapani, J. L. Prince, and R. H. Taylor, "Atlas-assisted tomography: Registration of a deformable atlas to compensate for limited-angle cone-beam trajectory," in *Proceedings of the IEEE International Symposium on Biomedical Imaging (ISBI)*, 2006.
- [9] D. L. Pham, "Robust fuzzy segmentation of magnetic resonance images," in *Proceedings of the Fourteenth IEEE Symposium on Computer-Based Medical Systems (CBMS2001)*. 2001, pp. 127–131, IEEE Press.
- [10] D. Tosun, M. E. Rettmann, X. Han, X. Tao, C. Xu, S. M. Resnick, D. L. Pham, and J. L. Prince, "Cortical surface segmentation and mapping," *NeuroImage Special Issue on IPAM Mathematics in Brain Imaging*, vol. 23(S1), pp. S108–S118, 2004.
- [11] W. L. Briggs, van E. Henson, and S. F. McCormick, *A Multigrid Tutorial, 2nd Edition*, SIAM, Philadelphia, PA, 2000.